

Uncertainty Evaluation of an In-Flight Absolute Radiometric Calibration Using a Statistical Monte Carlo Method

Wei Chen, Haimeng Zhao, Zhanqing Li, Xin Jing, and Lei Yan, *Senior Member, IEEE*

Abstract—The absolute radiometric calibration of remote sensing sensors is crucial to the accurate retrieval of biogeophysical parameters through remote sensing. The radiometric calibration uncertainty is the index that describes the reliability of a calibration result and is usually empirically determined by assuming that all of the factors involved are independent of each other. Through a field campaign carried out in Inner Mongolia, China, which aimed to accurately calibrate remote sensing sensors, we developed a Monte Carlo method that statistically evaluates the radiometric calibration uncertainty. From Monte Carlo simulations, it was revealed that the overall uncertainty is much smaller than the root sum of squares of each factor, suggesting that there is some negative correlation among some of the factors. For a surface with a low reflectance ($\sim 5\%$), the radiometric calibration uncertainty was $\sim 7.0\%$, whereas for a surface with a reflectance larger than 20% , the uncertainty was stable at $\sim 3.0\%$. This result suggests that the quality of remote sensing data should be carefully examined for surfaces with a low reflectance.

Index Terms—Radiometric calibration, radiometric targets, reflectance-based method, uncertainty.

I. INTRODUCTION

THE in-flight radiometric calibration of a remote sensing sensor is a critical activity that must be carefully performed so that remotely sensed data have high enough accuracy to be used in the retrieval of biogeophysical parameters [1]–[3]. The reliability of the absolute radiometric accuracy of remotely sensed data is directly relevant to the accuracy of the retrieval of important biogeophysical quantities, such as aerosol optical depth (AOD) [4], surface albedo, and vegetation index. Increasing the reliability requires a substantially improved knowledge of

the uncertainty of the absolute radiometric calibration for each band of the sensor.

In-flight absolute radiometric calibration is a highly reliable vicarious calibration method that depends on in situ measurements of surface and atmospheric parameters [5]. During the in situ measurement, the surface reflectance, aerosol optical properties, water vapor content, and ozone content are measured, as mentioned in [2], [3], and [6]–[8]. The reflectance-based method is widely used for calibrating remote sensing sensors with high accuracy, such as the Enhanced Thematic Mapper Plus (ETM+) [7], IKONOS [9], the Moderate Resolution Imaging Spectroradiometer (MODIS), and the Multi-angular Imaging Spectroradiometer [10].

The radiometric calibration uncertainty is a key index describing the reliability of a calibration result. The lower the uncertainty, the more reliable the result and the closer it is to the true value. The uncertainty of the reflectance-based method is normally estimated from a composite of the separate factors that contribute to the overall uncertainty, such as surface reflectance, aerosol properties, ozone content, and water vapor content.

Due to the nonlinearity of the radiative transfer equation, it is almost impossible to directly retrieve the in-flight absolute radiometric calibration uncertainty through radiative transfer calculations. Instead, the uncertainty for each factor involved in the measurement is empirically estimated. These factors are assumed to be independent of each other, and the overall uncertainty is the root sum of squares of the uncertainty of each factor [6]. An uncertainty of approximately 5% is estimated for the reflectance-based method [11], [12]. Another effort to estimate the uncertainty of the cross-calibration between a highly accurate sensor and a sensor with low accuracy involves the use of pseudoinvariant calibration sites, which results in an uncertainty of 5% or less [13], [14]. However, this approach highly depends on the accuracy of the highly accurate sensor used as a standard benchmark. For example, MODIS with relatively high accuracy is used as a reference standard for the Advanced Very High Resolution Radiometer. Furthermore, the factors involved, such as AOD and surface reflectance, are not independent of each other, indicating that one factor may increase or decrease the uncertainty brought on by other factors. For example, an increase in the surface reflectance would decrease the amount that atmospheric aerosols contribute to the apparent radiance. A relatively small variation in AOD would not change the apparent radiance significantly when surface reflectance is high. For a surface with a low reflectance, the

Manuscript received November 26, 2013; revised July 29, 2014 and September 21, 2014; accepted October 23, 2014. This work was supported in part by the National High Technology Research and Development Program of China under Grant 2008AA121806, by the National Natural Science Foundation of China under Grant 41171306, and by the Fundamental Research Funds for the Central Universities under Grant 2014QD02.

W. Chen is with the College of Geoscience and Surveying Engineering, China University of Mining and Technology, Beijing 100083, China (e-mail: chenw@cumt.edu.cn).

H. Zhao, X. Jing, and L. Yan are with the Institute of Remote Sensing and Geographic Information System, Peking University, Beijing 100871, China (e-mail: liyan@pku.edu.cn).

Z. Li is with the Earth System Science Interdisciplinary Center, University of Maryland, College Park, MD 20742 USA.

Color versions of one or more of the figures in this paper are available online at <http://ieeexplore.ieee.org>.

Digital Object Identifier 10.1109/TGRS.2014.2366779

TABLE I
MAIN RADIOMETRIC TEST FIELDS LOCATED AROUND THE WORLD

| Name | Geographic Location | Latitude (°) | Longitude (°) | Elevation (m) | Area (km ²) |
|-------------------------|--|--------------|---------------|---------------|-------------------------|
| White Sands | New Mexico USA | + 32. 23 | -106. 28 | 1196 | 40×40 |
| Chuck Site, White Sands | New Mexico, USA | + 32. 92 | - 106. 35 | 1196 | 0. 5×0.5 |
| Railroad Valley Playa, | Central Nevada, USA | + 38. 48 | - 115. 66 | 1435 | 10×10 |
| Lunar Lake Playa | Nevada, USA | + 38. 40 | - 115. 99 | 1750 | 1. 5×2.5 |
| Ivanpah Playa, | Nevada California, USA | + 35. 50 | - 115. 40 | 242 | 5× 5 |
| Rogers Dry Lake | Edwards Air Force Base, California, USA | + 34. 96 | - 117. 86 | 694 | 1 ×2 |
| Newell County | Rangeland, Alberta, Canada | + 50. 30 | 111. 64 | 750 | 7 ×7 |
| Tinga Tingana | Strzelecki Desert, South Australia, Australia | - 29. 00 | +139. 83 | 100 | 19×19 |
| Uardry, Hay | New South Wales, Australia | - 34. 39 | +145. 31 | 94 | 2× 2 |
| Lake Frome | Australia | - 30. 8 | +139. 65 | 0 | 10×10 |
| La Crau | France | + 43. 55 | + 4. 87 | 20 | 2 ×2 |
| Dunhuang | China | + 40. 20 | + 94. 43 | 1160 | 25×25 |

atmospheric contribution to the apparent radiance dominates; thus, a tiny change in AOD would change the apparent radiance greatly in terms of percentage.

However, this type of effect, where uncertainties are different with different surface reflectance, could not be directly predicted by both empirical and pseudoinvariant methods. In this paper, a statistical Monte Carlo method is proposed to estimate the uncertainty of the absolute vicarious calibration. The uncertainties brought by the AOD, surface reflectance, aerosol model, water vapor content, and ozone content are all simulated through statistical analysis. The overall uncertainty is also calculated through this numerical method instead of a root sum squares method.

A field campaign was carried out on November 14, 2010, in Inner Mongolia for the purpose of accurately calibrating the sensor onboard an unmanned aerial vehicle (UAV). As part of the calibration exercise, a set of well-designed radiometric targets possessing reasonably good Lambertian surfaces was deployed. During the campaign, target reflectance, AOD, and water vapor content were measured. The ozone column amount was obtained from the Ozone Monitoring Instrument (OMI) daily $1^\circ \times 1^\circ$ ozone content product. The Second Simulation of a Satellite Signal in the Solar Spectrum (6S) was used as the radiative transfer model to compute the apparent radiance. In our campaign, the calibration result reveals that the overall uncertainty is much smaller than the root sum squares of each single uncertainty, suggesting that there is some type of negative correlation among some factors.

The main objectives of this paper are to present a Monte Carlo statistical method to estimate the overall absolute radiometric calibration uncertainty and to understand the relationship between the uncertainties brought on by various factors and the overall uncertainty. This paper is structured as follows. Descriptions of the test field and instruments (including the

sensor and targets) are introduced in Section II. Section III describes the radiometric calibration method, the data collecting process, and the Monte Carlo method. Section IV presents the uncertainty estimates of the separate factors and the overall uncertainty estimate, as well as an analysis of the relationship between the two. Conclusions are given in Section V.

II. DESCRIPTION OF TEST FIELD AND INSTRUMENTS

A. Test Field

Since the 1970s, radiometric calibration test fields have been established around the world to provide accurate calibration for a series of satellite sensors, such as the ETM+ and the Système Pour l'Observation de la Terre [7], [15]; Table I lists the major test fields. These fields consist of natural surfaces with a relatively smooth reflectance spectrum suitable for the calibration of spaceborne sensors. However, there are few test fields suitable for the calibration of airborne sensors, which have higher spatial resolutions (e.g., ~ 1 m). The ideal test field for this purpose requires a location that has generally stable weather conditions (for safe aircraft take off and landing) and low aerosol loading. In China, over two thirds of remotely sensed data are collected by airborne sensors rather than satellite sensors; thus, there is a great need for proper calibration test fields. To meet this urgent demand, such a test field was constructed in Bayannur, Inner Mongolia, China.

A map of the terrain and boundaries of the test field is shown in Fig. 1. The test field itself covers an area of 292.5 km² and is mainly covered by a smooth expanse of grass. Weather conditions tend to be dry, with little precipitation throughout the year. The annual maximum temperature is approximately 38 °C in the summer, and the minimum temperature is around -30 °C in wintertime. The expectancy of clear weather is high for this

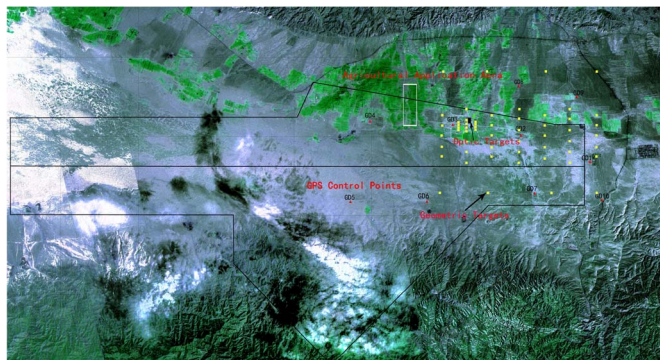


Fig. 1. Map of the calibration test field area and location of the targets (red dots are the GPS control points; yellow points are the geometric targets for geometric correction not shown in this paper; the small black rectangle is the optic targets area).

region. The area in the green line is the aviation area for our test field; the natural targets and area for agriculture application located in the northern area of our test field are shown as the white rectangle area. There is also a meteorological station here for monitoring the weather conditions. GPS control points were deployed a year ahead of the construction of the test field, promising an accurate geometric calibration for the images.

B. Test Field Targets

In addition to natural targets with a relatively smooth reflectance spectrum, artificial optical targets are designed and deployed for both geometric and radiometric calibration purposes. The following five classes of targets were deployed in the test field (see Fig. 2).

- 1) Resolution bar targets, noted as TX in Fig. 2: This type of target array consists of a series of targets with resolutions ranging from 0.05 to 1.1 m. Resolution bar targets are used for geometric calibration and determining the modulation transfer function.
- 2) Siemens star target, noted as SX in Fig. 2: This type of target combines a small triangle with trapezoidal targets to detect the resolution of a sensor. The central angle of the Siemens star target is 110° , and its radius is 46.4 m.
- 3) Radiometric characteristic targets, noted as F* in Fig. 2: This type of target has a relatively smooth spectrum in the spectral range of 400–1000 nm, which is the imaging range of the sensor in this paper. It is used for radiometric calibration, and the target surface is as Lambertian as possible in design. The size of F04 and F60 is $20\text{ m} \times 20\text{ m}$, whereas the size of the rest of the radiometric calibration targets is $15\text{ m} \times 15\text{ m}$.
- 4) Hyperspectral validation targets, noted as CH* in Fig. 2: This type of target contains peaks in the spectral range of 400–1000 nm, which are used to validate errors brought on by radiometric calibration. The size of these targets is $15\text{ m} \times 15\text{ m}$.
- 5) Multispectral evaluation targets, noted as C* in Fig. 2: This type of target is used for evaluating the spectral performances of sensors. The size of these targets is $7\text{ m} \times 7\text{ m}$.

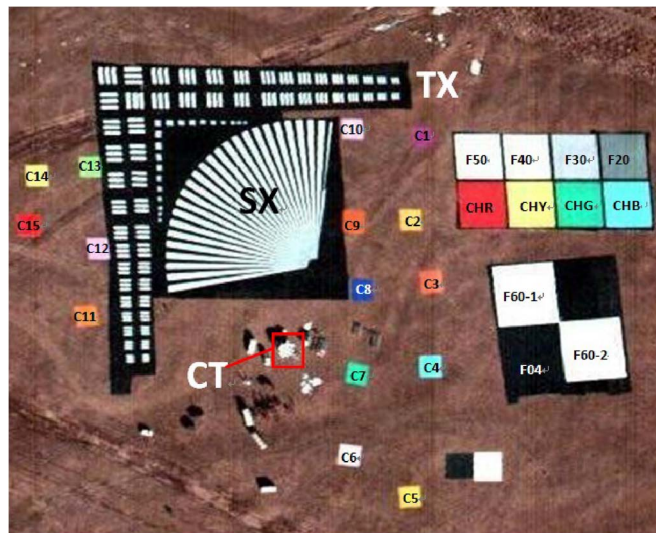


Fig. 2. Photograph of the targets taken from the hyperspectral imager on November 14, 2010. F04, F20, F40, F50, and F60 are the targets used for the radiometric calibration; C1–C15 are the multispectral evaluation targets; CHR, CHY, CHG, and CHB are the radiometric validation targets used to validate the results from the radiometric calibration; SX, TX, and CT are the targets used for the geometric calibration.

In this paper, radiometric characteristic targets are used and analyzed. The analysis of data from other targets is not included in this paper.

C. WVMI

Three optical sensors were installed on board the UAV: 1) a multispectral line scan sensor, or wide-view multispectral imager (WVMI), with four multispectral bands and one panchromatic band; 2) a hyperspectral line scan sensor with 128 bands ranging in wavelength from 400 to 1030 nm, at an average spectral resolution of approximately 6 nm; and 3) a small plane array sensor for geometric calibration. This paper focuses on the radiometric calibration and uncertainty of the WVMI.

The imager, a line scan charge-coupled device sensor, was designed and manufactured by the Changchun Institute of Optics, Fine Mechanics and Physics, Chinese Academy of Sciences. The swath of the WVMI covers approximately 6 km at a cruising height of 5 km; the spatial resolution of the WVMI is 1 m for the multispectral bands and 0.5 m for the panchromatic band at this cruising height. The spectral ranges of the four multispectral bands and the panchromatic band are listed in Table II, and the spectral response functions of the four multispectral bands are shown in Fig. 3.

III. METHODOLOGY

A. Radiometric Calibration Method

The reflectance-based method was used to calibrate the WVMI. Surface reflectance and various atmospheric parameter measurements were input into a radiative transfer model (the 6S model) to calculate the apparent radiance at the sensor level, which was then compared with the response reported by the

TABLE II
SPECTRAL BAND RANGES OF MULTISPECTRAL SENSOR

| Band | Blue (nm) | Green (nm) | Red (nm) | Infrared (nm) | Pan (nm) |
|----------------|--------------|---------------|-------------|------------------|----------|
| Spectral Range | 420~520 | 520~600 | 630~690 | 760~900 | 475~750 |

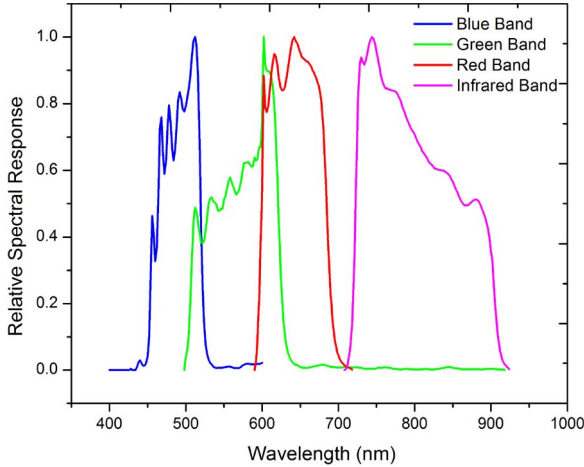


Fig. 3. Spectral response functions of the four multispectral bands.

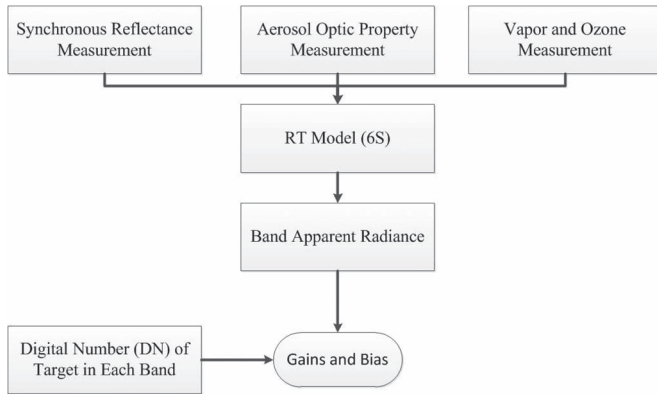


Fig. 4. Flowchart outlining the steps taken in the reflectance-based method.

sensor. A flowchart of the steps taken is given in Fig. 4. Details of the reflectance-based method can be found in [2], [5], [7], [13], and [14]. Previous studies using such a reflectance-based method to estimate apparent radiance relied on measurements from uniform surfaces with relatively high reflectances. Under this condition, the gain and bias coefficients may not reflect the actual relationship between the sensor output and the energy it receives. During the field campaign, a set of radiometric characteristic targets possessing different reflectances (4%, 20%, 30%, 40%, 50%, and 60%) was designed and deployed to get a better estimate of the radiometric calibration equation.

The relationship between apparent radiance, i.e., L^* , and output from the sensor, or digital number, i.e., DN, in a particular band is given by

$$L^* = a * DN + b \tag{1}$$

where a is the gain coefficient, and b is the bias coefficient. The least squares method is used to obtain the best fit between L^*

and DN for each band, which is expressed as follows:

$$a = \frac{(\sum L_i^*)}{n} - \frac{b(\sum DN_i)}{n} \tag{2}$$

$$b = \frac{n \sum L_i^* DN_i - \sum L_i^* \sum DN_i}{n \sum DN_i^2 - (\sum DN_i)^2} \tag{3}$$

where n is the number of targets used for the radiometric calibration, DN_i is the DN of the i th target, and L_i^* is the apparent radiance calculated from the radiative transfer model for the i th target.

B. Measurement of Target Reflectance

Surface reflectance is an important source of calibration uncertainty [6], mainly due to the bidirectional reflectance properties of a surface. Ideally, strictly synchronous measurements of reflectance from all targets should be made at the time of the UAV overpass. However, this was an unrealistic goal during the field campaign because there were, in total, 26 radiometric targets spread out over the test field. To minimize this uncertainty, reflectance measurements over the set of near-Lambertian targets (see Fig. 5 for details) were taken nine times within a period of 3 min; two extra measurements were made over the reference board to ensure the quality of the data. During this field campaign, surface reflectance data were collected using an ASD spectrometer set to the radiance mode (spectral range of 400–2500 nm); the reference board was calibrated before the campaign. The average reflectance of each target, i.e., $\bar{\rho}$, is calculated using the following equation:

$$\bar{\rho} = \frac{\overline{G}_\lambda}{\overline{P}_\lambda} * B(\theta, \lambda) \tag{4}$$

where \overline{G}_λ is the average response of the target measurement, \overline{P}_λ is the average response of the reference board measurement, and $B(\theta, \lambda)$ is the directional reflectance parameter of the reference board. The reflectances of the radiometric calibration targets are shown in Fig. 6. Measurements were taken between 10:20 and 11:20 (local time); the solar zenith angle varied from 66° to 58° during this period. The mean errors brought on by variations in the incident angle for targets with nominal reflectances of 4% and 60% (denoted by F04 and F60 in Fig. 2) are 4% and 1.7%, respectively (see Fig. 5). This suggests that the reflectances measured from the targets are reasonably accurate.

C. Measurement of Atmospheric Parameters

The reflectance-based radiometric calibration method used here requires information about the AOD, ozone content, water vapor content, and aerosol type. The AOD was measured once every 10–15 min during the day using three calibrated handheld

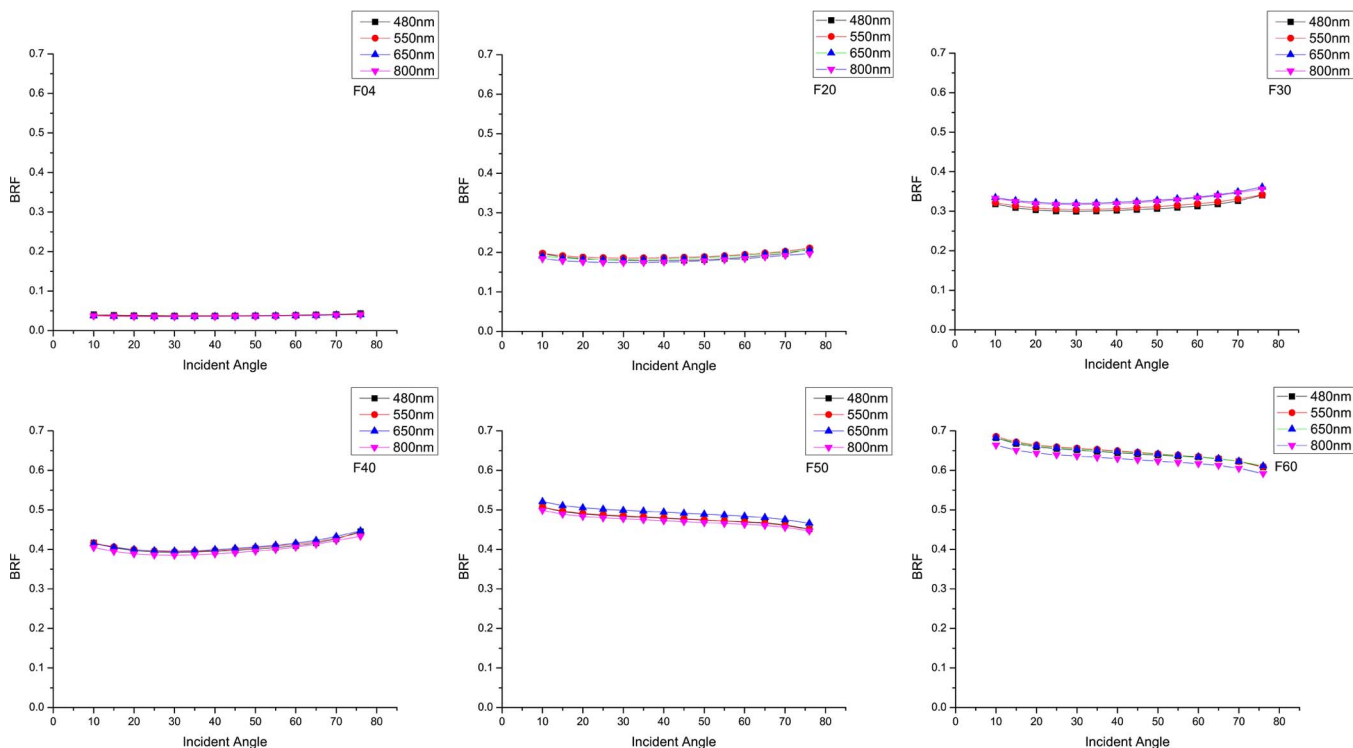


Fig. 5. Bidirectional reflectance factors of the six radiometric targets (denoted by F04, F20, F30, F40, F50, and F60) at four wavelengths (representing the center wavelengths of each band).

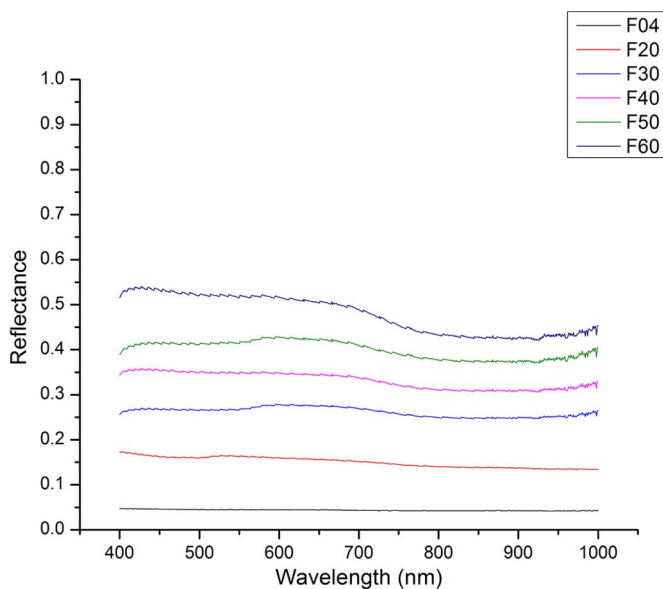


Fig. 6. Synchronous measurements of reflectance over the six targets during the campaign.

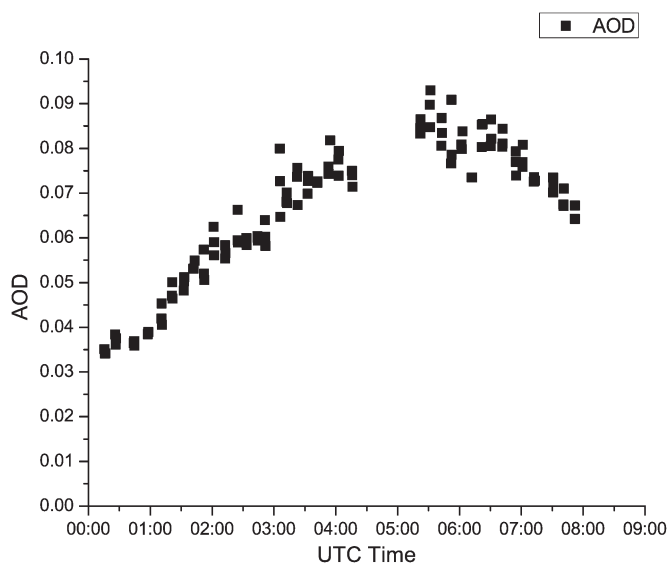


Fig. 7. Time series of the AOD during the campaign.

Microtops II Sun photometers; the time series of the AOD is shown in Fig. 7. Note that the atmosphere is pristine with a mean AOD value of 0.075. A break was taken around noontime to change personnel; thus, there is a gap in the measurements at that time. The field campaign was not set up to analyze the physical and chemical nature of the aerosols present; thus, an assumption about the aerosol model had to be made. Given that the test field borders the Gobi Desert and is not affected by the warm and humid air from the sea located to the southeast, a con-

tinental aerosol model composed of three different components with lognormal distributions was assumed. The uncertainty of this assumption will be discussed in a later section. The OMI provided the ozone content, and the water vapor content was derived from balloon soundings.

D. Description of the Statistical Monte Carlo Method

The Monte Carlo method is a computational algorithm that relies on random and repeated sampling to obtain approximate results. This method can provide numerically approximate

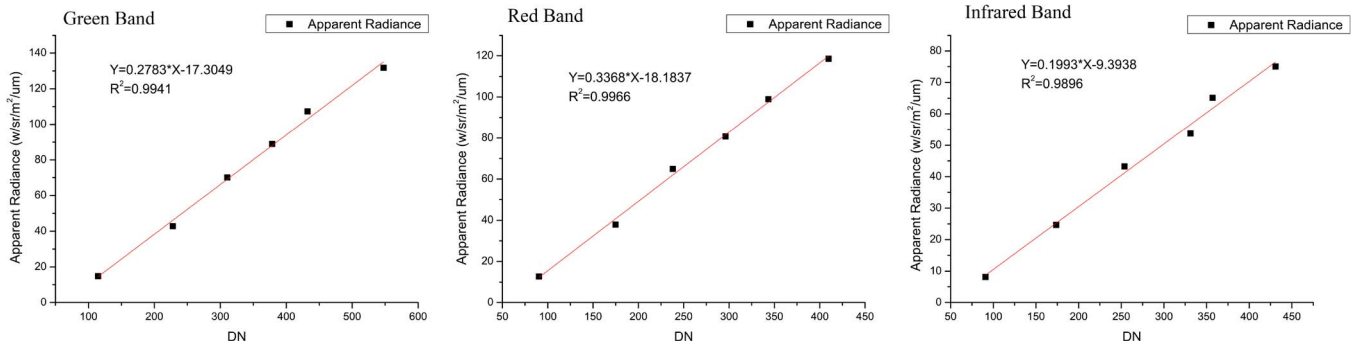


Fig. 8. Calibration results from the (left) green, (middle) red, and (right) infrared bands.

solutions to problems without analytical solutions, such as the problem of estimating the uncertainty involved with absolute radiometric calibration. This method was used here to randomly sample the various factors (surface reflectance, AOD, aerosol model, water vapor content, and ozone content) within their respective error ranges and following some probability distribution for input into a radiative transfer model. The model was run repeatedly using these randomly sampled input parameters so that the variance of the simulated apparent radiance could be determined. The number of simulations to perform is an important aspect of the Monte Carlo method. Too few simulations would not reflect the true variance of the simulated apparent radiance, and too many simulations would be computationally burdensome. A sensitivity study was performed, and 1000 simulations were deemed sufficient for obtaining stable statistical results.

It was first analyzed which error distribution model is suitable to describe the measurement results to derive the uncertainty estimation for each factor. For surface reflectance, the measurement errors were less than 3% in most cases, except for the target with a nominal reflectance of 4% (target F04). For aerosols, we compared the standard deviation of measurements taken before and after the UAV overpass; the standard deviation was 0.002 with an average AOD of 0.075. As a further constraint, we took into account the accuracy of the Sun photometers used to measure the AOD; the instrument error is better than 0.04. The latter value, which is larger, was used as input for the Monte Carlo simulations. Two aerosol models were considered representative of the range of aerosols possibly present over the test field, namely, a continental aerosol model and the Beijing model suggested by [16], which is based upon Monte Carlo simulations made using clear-sky information as input. The former model consists of three components, where the weighted volume percentages of each component are 70% (dust), 29% (water soluble), and 1% (soot); the weighted volume percentages of each component in the latter model are 36% (dust), 63% (water soluble), and 1% (soot). Given that there is little anthropogenic pollution in the area, the volume percentage of soot was set at 1% in the aerosol model used for the simulations; the volume percentages of dustlike and water-soluble components were evenly split between the continental and Beijing models. The uncertainties associated with the measurements of water vapor and ozone content were 0.1 g/cm² and 2%, respectively. After determining the uncer-

tainty of each factor, a root sum of squares overall uncertainty was calculated. In addition, for comparison purposes, statistically derived overall uncertainties were obtained using the Monte Carlo method.

IV. RESULTS AND DISCUSSION

During the field campaign that took place on November 14, 2010, the reflectance spectra of the six radiometric calibration targets were measured, and the results are shown in Fig. 6; there is little variation in the spectra of each band. The AOD during the campaign varied from 0.06 to 0.08 with an average of 0.075, as shown in Fig. 7, indicating a clean atmosphere. The water vapor content was approximately 0.102 g/cm² according to soundings immediately after the landing of the UAV. The reason for the clean and dry atmosphere is that, during the winter, northwesterly winds carry away most of the local aerosols and water vapor in the atmosphere. The ozone column amount on this day was 310 DU. Only green, red, and infrared bands were calibrated because the blue band failed to capture an image during the UAV overpass; Fig. 8 shows the results from the calibration. There is a strong linear correlation between the simulated apparent radiance and the digital output by the sensor ($R^2 \sim 0.99$), indicating that the linear response of the WVMI is very good.

A. Uncertainty of Each Factor

1) *Reflectance*: Surface reflectance is one major source of uncertainty. In the field experiment, the error associated with reflectance measurements is $\sim 3\%$ in all cases, except for measurements from the F04 target, which has a nominal reflectance of 4%. This is because a minor absolute error in the measurement of reflectance from this target will result in a high relative error.

In preparation for the campaign, the ASD spectrometer and the reference board were carefully calibrated in a laboratory; the radiometric calibration targets were stored in a clean warehouse under dry ambient conditions. To quantify the overall uncertainty brought on by the uncertainty in reflectance measurements, we assumed that reflectance follows a normal distribution with a standard deviation of 3% (reflectance $\sim N(r, \sigma^2)$, $\sigma = 0.03$). The mean reflectances measured over each radiometric calibration target are given in Table III. Fig. 9 shows how

TABLE III
MEAN REFLECTANCE OF EACH RADIOMETRIC CALIBRATION TARGET IN DIFFERENT BANDS

| | Green Band | Red Band | Infrared Band |
|-----|------------|----------|---------------|
| F04 | 0.044 | 0.044 | 0.042 |
| F20 | 0.161 | 0.157 | 0.142 |
| F30 | 0.272 | 0.275 | 0.253 |
| F40 | 0.348 | 0.345 | 0.315 |
| F50 | 0.421 | 0.423 | 0.382 |
| F60 | 0.516 | 0.507 | 0.441 |

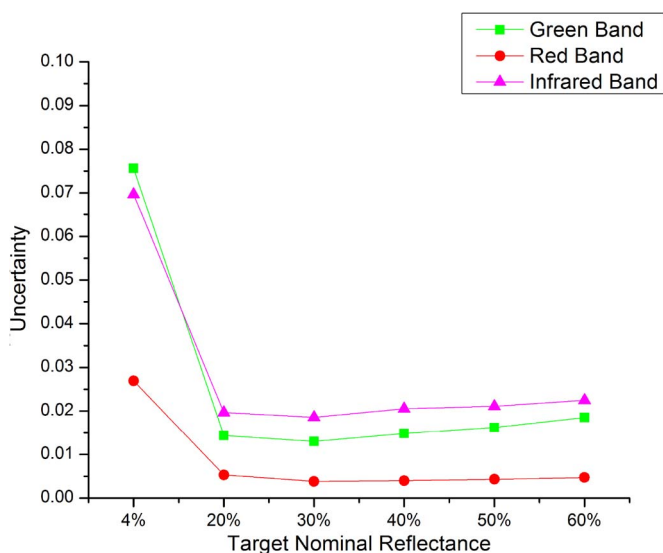


Fig. 9. Calibration uncertainty brought on by the uncertainty in reflectance measurements. The *x*-axis represents the target nominal reflectance, which is slightly different from the real surface reflectance.

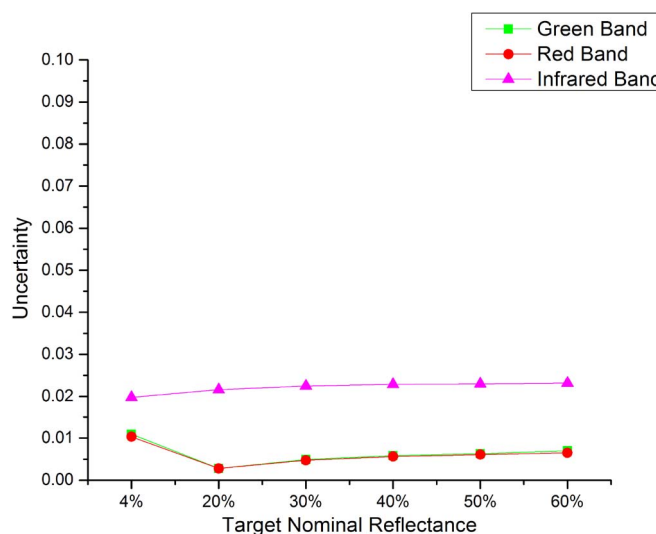


Fig. 10. Calibration uncertainty brought on by the uncertainty in the AOD measurements.

the uncertainty in the radiometric calibration arising from the uncertainty in surface reflectance changes with varying surface reflectances in different bands. When the surface reflectance is very low (~4.0%), the uncertainty in reflectance measurements will bring about large errors in the calibration; the errors are 7.5%, 3%, and 6.9% in the green, red, and infrared bands, respectively. However, as the surface reflectance increases to greater than 20.0%, the uncertainty brought on by reflectance measurements drops sharply to approximately 1.5% for the green band, 0.5% for the red band, and 2% for the infrared band.

2) *AOD*: Aerosols in the atmosphere have large spatial and temporal variations, which can modify the apparent radiance the WVMi receives. The aerosol loading was low during the field campaign (~0.075). The handheld Sun photometer used to measure the AOD has an error of 0.04, according to the manufacturer. In our Monte Carlo simulations, the AOD varied from 0.035 to 0.115 and was normally distributed. Fig. 10 shows that the overall uncertainty brought by uncertainties in the AOD measurements is generally smooth for each target in the three bands. This indicates that the contribution from aerosols toward the overall calibration uncertainty is relatively stable during the campaign. The largest uncertainty is seen in the infrared band (~2%), whereas the uncertainties in the green and red bands are as low as 0.5%. The reason for this is that the signal of the infrared band is relatively lower than that of the

green and red bands; a small absolute variation will result in a high relative uncertainty.

3) *Aerosol Model*: The choice of aerosol model, which sets the single scattering albedo, asymmetry factor, and extinction coefficient of aerosols in different bands, is another major source of uncertainty in radiometric calibration. In 6S, there are mainly three ways to describe aerosol models. The first one is to use precalculated models that are mainly derived from laboratory measurements, such as the biomass model and the desert model. The second one is calculated from MIE code. For example, oceanic, dust, and soot models are all calculated from MIE code by setting refractive indices at different bands and size distributions. We can also set our own parameters to run MIE code inside 6S to calculate a new aerosol model by setting the refractive index and size distributions (starting and ending wavelength and size distribution function such as lognormal or gamma distribution). The third one is to use Sun photometer measurements to retrieve the volume distributions of aerosol particles. However, due to the equipment limitation, our Sun photometer, Microtops, is unable to record the size distribution of aerosol particles. In this paper, MIE code calculation combinations are used to model the distributions of aerosol particles.

We assumed a continental aerosol model consisting of three externally mixed aerosol components having lognormal distributions, namely, a dustlike component (70%), a water-soluble component (29%), and a soot component (1%), as recommended by the WMO-WCP112.

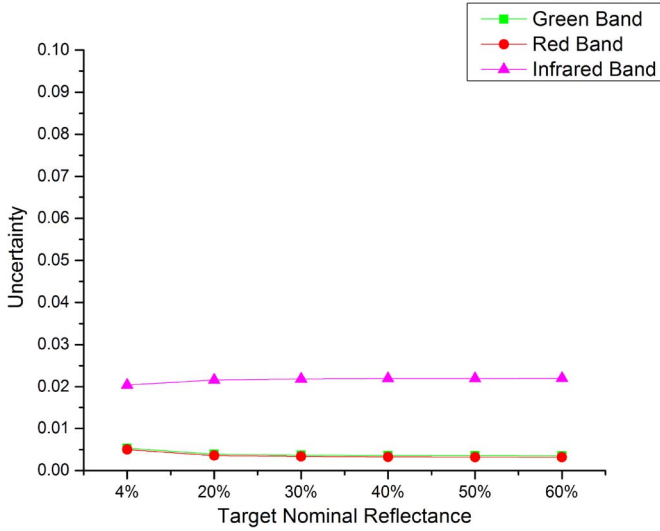


Fig. 11. Calibration uncertainty brought on by the uncertainty in the choice of aerosol model.

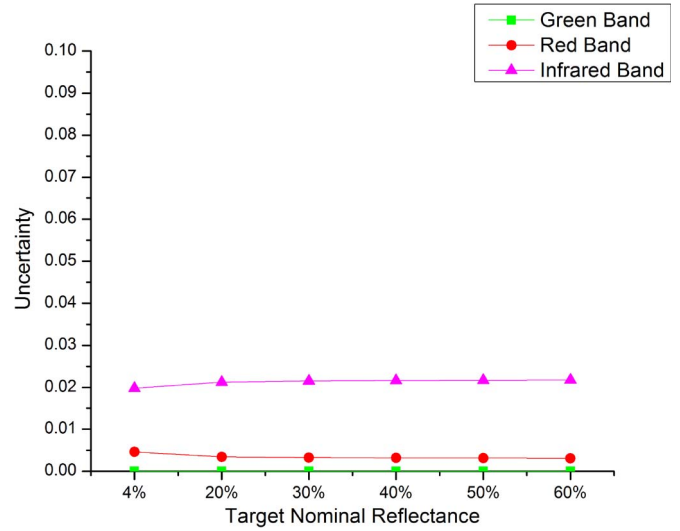


Fig. 12. Calibration uncertainty brought on by the uncertainty in the water vapor content measurements.

Given the climate of Inner Mongolia, we assumed that the aerosol composition falls somewhere between the Beijing aerosol model (dustlike: 36%, water soluble: 62%, soot: 1%) [16] and the continental model. Different aerosol model formulations were used in the Monte Carlo simulations, and the results are shown in Fig. 11. The uncertainty brought on by the choice of aerosol model is relatively stable in all three bands. The infrared band has the largest uncertainty ($\sim 2\%$), which suggests that large aerosol particles may have been present during the campaign; the uncertainties in the green and red bands are as low as 0.5%.

4) *Water Vapor*: The water vapor content is measured using balloon-borne radiosondes; these measurements have an uncertainty of 0.1 g/cm^2 . During the field campaign, the prevailing northwesterly winds were cold and dry; thus, the water vapor content was very low ($\sim 0.102 \text{ g/cm}^2$). For the Monte Carlo simulations, the normally distributed water vapor content varied from 0.01 to 0.202 g/cm^2 ; the results are shown in Fig. 12. The uncertainties in the overall calibration due to uncertainties in the measurements of water vapor content in the green band are almost zero; uncertainties reach $\sim 2\%$ in the other bands, which are located closer to water vapor absorbing bands ($0.905 \mu\text{m}$).

5) *Ozone Content*: The ozone column amount is obtained from the $1^\circ \times 1^\circ$ OMI product; these measurements have an uncertainty of $\sim 2\%$. Uncertainties in the overall calibration due to this uncertainty in the measurements of ozone content are shown in Fig. 13; they are almost zero in the green and red bands and reach 2% in the infrared band.

6) *Overall Uncertainty Including All Factors*: A common assumption made when calculating the overall uncertainty of a radiative calibration is that the contributions of each factor to the calibration are independent from each other. Then, the overall uncertainty, i.e., σ_o , is the root sum of squares of the uncertainties of all of the factors, i.e.,

$$\sigma_o = \sqrt{\sigma_{\text{ref}}^2 + \sigma_{\text{AOD}}^2 + \sigma_{\text{AM}}^2 + \sigma_{\text{water}}^2 + \sigma_{\text{ozone}}^2} \quad (5)$$

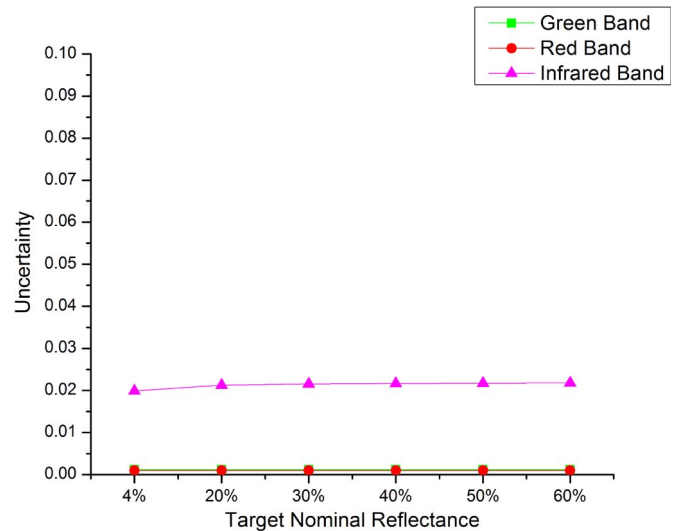


Fig. 13. Calibration uncertainty brought on by the uncertainty in the ozone column amount from OMI.

where σ_{ref} is the uncertainty in the surface reflectance measurements, σ_{AOD} is the uncertainty in the AOD measurements, σ_{AM} is the uncertainty due to the choice of aerosol model, σ_{water} is the uncertainty in the water vapor measurements, and σ_{ozone} is the uncertainty in the ozone content measurements.

However, the factors included here are not truly independent of each other. For example, the AOD is deeply affected by the choice of aerosol model because the model defines the size distribution and the single scattering property of aerosols. In addition, increasing or decreasing the surface reflectance may affect the radiance reflected by aerosols. Thus, the overall uncertainty should include some measure of covariance between each pair of factors. This was done in a new set of Monte Carlo simulations using variations of the five factors as input and following the same distribution mentioned in Section IV. Fig. 14 shows the total uncertainty in each band. It should be noted

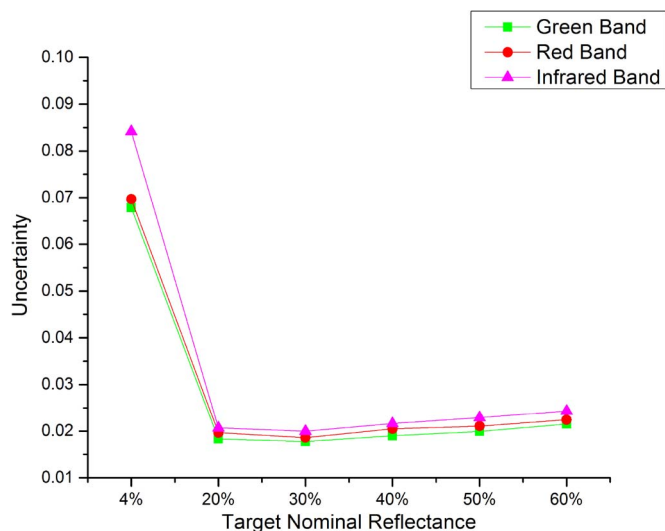


Fig. 14. Overall calibration uncertainty.

that the total uncertainty calculated using the Monte Carlo method is smaller than that calculated using (5), indicating that there is some type of counterbalance between some factors included in our analysis. When the surface reflectance is low, for example, approximately 4.0%, the calibration uncertainty is very high because the contribution from the atmosphere dominates. The target with a nominal reflectance of 4% has uncertainties ranging from 7.0% to 9.0% in all three bands. All of the other targets have relatively stable uncertainties ranging from 2.0% to 3.0%. Among the three bands, the green band has the lowest uncertainty because the aerosol loading was low during the campaign; the infrared band has the largest uncertainty. In general, the results from the calibration are very good.

For further discussion of low-reflectance situations, a sensitive experiment is carried out to demonstrate that low-reflectance situations may have the largest relative error. In this experiment, the continental and Beijing aerosol models are chosen as the two aerosol models. Surface reflectance ranging from 0.01 to 0.2 is chosen to explain low-surface-reflectance situations. The result is shown in Fig. 15. When surface reflectance increases from 0.01 to 0.2, the absolute radiance difference of two simulations increases from 0.13 to 0.43 $\text{W}/\text{sr}/\text{m}^2/\mu\text{m}$. Meanwhile, the relative difference of the two simulations decreases from 0.02 to 0.008. This indicates that, for low-reflectance situations (reflectance lower than 5%), the atmosphere contribution is high (67% when reflectance is 1% and 38% when reflectance is 4%), and the difference between the different simulations may gather a relatively large relative error. This is also true for uncertainty, which is described as the standard deviation of the calibration results. However, because of a lack of targets with reflectance ranging from 4% to 20%, it is hard to discern which reflectance range is affected most by the atmosphere and with highest uncertainty. Considering that our targets' lowest reflectance is approximately 4%, we could infer that, when the reflectance is lower than 4%, the uncertainty of the calibration result may be high due to a low signal-to-noise ratio. Under these circumstances,

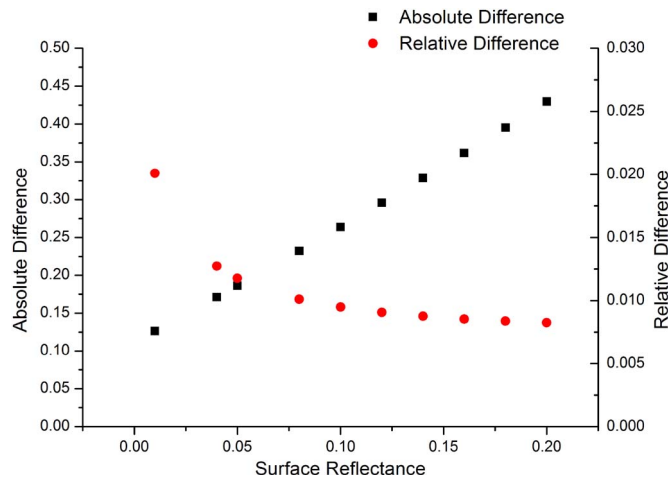


Fig. 15. Relative and absolute differences between surface reflectance situations for two different aerosol models in the green band. (Note that the difference is not the uncertainty; uncertainty is the standard deviation between the true value and the calculated value).

the quality of the remote sensing data and product should be carefully examined.

V. CONCLUSION

A field campaign was carried out on November 14, 2010, in Inner Mongolia for the purpose of accurately calibrating the sensor on board an UAV. As part of the calibration exercise, a set of well-designed radiometric targets possessing reasonably good Lambertian surfaces was deployed. We used a Monte Carlo method to calculate the individual uncertainties brought on by the surface reflectance, AOD, aerosol model, water vapor measurement, and ozone content measurement. Each factor, subject to particular probability distributions, was input into a radiative transfer model, and repeated simulations of the apparent radiance were made. The results reveal that the overall uncertainty when using the Monte Carlo method is smaller than that calculated using the root sum of squares, indicating that some of the factors included in the analysis have a negative effect on other factors.

The radiometric calibration results show that, for a surface with low reflectance, the uncertainty of radiometric calibration reaches 7.0%–9.0%. The reason for this result may be that, under this circumstance, the surface contribution is very small, while the main signal the sensor receives comes from the atmosphere. When the surface reflectance increases to more than 20.0%, the total uncertainty of the radiometric calibration drops to the 2.0%–3.0% level. The green band, where aerosols have the greatest effect, has the lowest total uncertainty. This is likely because the aerosol loading during the field campaign was very low. The infrared band has the largest uncertainty. The total uncertainties of all three bands are smaller than 4.0% for surface reflectances greater than 20.0%. For a surface reflectance of 4.0%, the radiometric calibration uncertainty can reach 7.0%, which suggests that, when using remotely sensed data measured over an area with low reflectance, the quality of these data should be examined before any potential application.

REFERENCES

- [1] D. Naughton *et al.*, "Absolute radiometric calibration of the RapidEye multispectral imager using the reflectance-based vicarious calibration method," *J. Appl. Remote Sens.*, vol. 5, no. 1, Aug. 12, 2011.
- [2] P. N. Slater *et al.*, "Reflectance-based and radiance-based methods for the in-flight absolute calibration of multispectral sensors," *Remote Sens. Environ.*, vol. 22, no. 1, pp. 11–37, Jun. 1987.
- [3] K. J. Thome, "Absolute radiometric calibration of Landsat 7 ETM+ using the reflectance-based method," *Remote Sens. Environ.*, vol. 78, no. 1, pp. 27–38, Oct. 2001.
- [4] Z. Li *et al.*, "Uncertainties in satellite remote sensing of aerosols and impact on monitoring its long-term trend: A review and perspective," *Ann. Geophys.*, vol. 27, no. 7, pp. 2755–2770, 2009.
- [5] K. J. Thome, K. Arai, S. Tsuchida, and S. F. Biggar, "Vicarious calibration of ASTER via the reflectance-based approach," *IEEE Trans. Geosci. Remote Sens.*, vol. 46, no. 10, pp. 3285–3295, Oct. 2008.
- [6] S. F. Biggar, P. N. Slater, and D. I. Gellman, "Uncertainties in the in-flight calibration of sensors with reference to measured ground sites in the 0.4–1.1 MU-M Range," *Remote Sens. Environ.*, vol. 48, pp. 245–252, May 1994.
- [7] K. J. Thome, D. L. Helder, D. Aaron, and J. D. Dewald, "Landsat-5 TM and Landsat-7 ETM+ absolute radiometric calibration using the reflectance-based method," *IEEE Trans. Geosci. Remote Sens.*, vol. 42, no. 12, pp. 2777–2785, Dec. 2004.
- [8] S. F. Biggar, R. P. Santerl, and P. N. Slater, "Irradiance-based calibration of imaging sensors," in *Proc. IEEE Int. Geosci. Remote Sens. Symp.*, College Park, MA, USA, 1990, pp. 507–510.
- [9] M. Pagnutti *et al.*, "Radiometric characterization of IKONOS multispectral imagery," *Remote Sens. Environ.*, vol. 88, no. 1/2, pp. 53–68, Nov. 2003.
- [10] K. Thome, S. Biggar, and H. J. Choi, "Vicarious calibration of Terra ASTER, MISR, and MODIS," in *Proc. Earth Observing Syst. IX*, vol. 5542, W. L. Barnes and J. J. Butler, Eds., 2004, pp. 290–299.
- [11] S. F. Biggar *et al.*, "Radiometric calibration of SPOT 2 HRV-A comparison of three methods," *Proc. SPIE*, vol. 1493, pp. 1–8, 1991.
- [12] C. J. Bruegge *et al.*, "The MISR radiometric calibration process," *Remote Sens. Environ.*, vol. 107, pp. 2–11, Mar. 2007.
- [13] D. L. Helder *et al.*, "Radiometric calibration of the Landsat MSS sensor series," *IEEE Trans. Geosci. Remote Sens.*, vol. 50, no. 6, pp. 2380–2399, Jun. 2012.
- [14] D. L. Helder *et al.*, "Updated radiometric calibration for the Landsat-5 thematic mapper reflective bands," *IEEE Trans. Geosci. Remote Sens.*, vol. 46, no. 10, pp. 3309–3325, Oct. 2008.
- [15] X. F. Gu, G. Guyot, and M. Verbrugge, "Evaluation of measurement errors in ground surface reflectance for satellite calibration," *Int. J. Remote Sens.*, vol. 13, no. 14, pp. 2531–2546, Sep. 1992.
- [16] T. Hong-zhao, Y. Lei, L. Cheng-cai, and G. Peng-qi, "Atmospheric correction for ETM+ imagery based on high resolution aerosol optical depth retrieved from MODIS data," *Geography Geo-Inf. Sci.*, vol. 26, pp. 12–17, 2010.



Wei Chen received the B.E. degree in geographical information system from Beijing Normal University, Beijing, China, in 2008 and the Ph.D. degree in photogrammetry and remote sensing from Peking University, Beijing.

He is currently a Lecturer with the College of Geoscience and Surveying Engineering, China University of Mining and Technology, Beijing. His major research interests include sensor calibration and atmospheric correction.



Haimeng Zhao received the B.E. degree in electrical engineering and automation from Beihang University (BUAA), Beijing, China, in 2004.

He is currently a Research Engineer with the Beijing Key Laboratory of Spatial Information Integration and 3S Engineering Applications, Peking University, Beijing. His major research interests include digital imaging, satellite sensor design, and optoelectronic instrument design.



Zhanqing Li received the B.Sc. and M.Sc. degrees from Nanjing Institute of Meteorology, Nanjing, China, and the Ph.D. degree from McGill University, Montreal, QC, Canada, in 1991.

Since 2001, he has been a Professor with the Department of Atmospheric and Oceanic Science and the Earth System Science Interdisciplinary Center, University of Maryland, College Park, MD, USA. He has engaged in a wide range of studies concerning climate change, atmospheric physics, and the terrestrial and atmospheric environment. He developed

a suite of remote sensing algorithms and generated products of surface and atmospheric radiation budget, photosynthetically active radiation, ultraviolet, cloud and aerosol parameters, precipitation, albedo, bidirectional reflectance distribution function, fire hotspots and burned areas, etc. He has led several major projects in the U.S. and China. To date, he has authored over 200 articles in leading journals, including *Nature*, *Science*, *Nature Geoscience*, *Proceedings of the National Academy of Sciences*, *Remote Sensing of the Environment*, and *Journal of Geophysical Research*, with a total citation of over 4800 and an h-index of 40.

Dr. Li was a President of the Chinese-American Oceanic and Atmospheric Association and a Fellow of the American Geophysical Union. He was also an Editor of the *Journal of Geophysical Research*. He has been a recipient of seven major awards, including the 2014 Yoram J. Kaufman Award.



Xin Jing received the B.E. degree in geomatics engineering from Tongji University, Shanghai, China, in 2007 and the M.E. degree in photogrammetry and remote sensing from Peking University, Beijing, China, in 2012. She is currently working toward the Ph.D. degree in photogrammetry and remote sensing at Peking University.

Her major research interests include hyperspectral remote sensing and remote sensing sensor calibration.



Lei Yan (SM'03) received the B.E. degree from the Nanjing University of Aeronautics and Astronautics, Nanjing, China, in 1982, the M.E. degree from the Navy University of Engineering, Nanjing, in 1989, and the Ph.D. degree from Tsinghua University, Beijing, China, in 1993.

From 1998 to 2000, he was a Full Professor and an Academic Leader of "One Hundred Famous Scientists' Plan" for the Chinese Academy of Sciences, Changchun Institute of Optics, Fine Mechanics and Physics, Chinese Academy of Sciences, Changchun,

China. Since 2001, he has been a Professor and the Head of the Beijing Key Laboratory of Spatial Information Integration and Its Applications, Institute of Remote Sensing and Geographic Information System, School of Earth and Space Sciences, Peking University, Beijing. He has authored four books, over 200 articles, and 14 patents. His major research interests include digital imaging, airborne remote sensing systems, and remote sensing image processing.

Dr. Yan was the recipient of the first award for Scientific and Technological Progress of Beijing City in 2012 for his contribution on the remote sensor development and its new discovery.